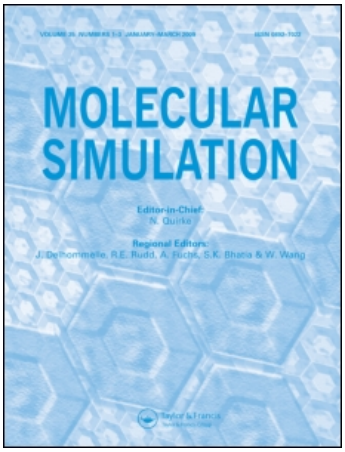

Molecular Simulation

Publication details, including instructions for authors and subscription information:
http://www.informaworld.com/smpp/title~content=t713644482

Electronic transport through a CNT-Pseudopeptide-CNT hybrid material

N. Bruque[a]; R. R. Pandey[a]; R. K. Lake[a]; H. Wang[b]; J. P. Lewis[b]
[a] Department of Electrical Engineering, University of California, Riverside, CA, USA [b] Department of Physics and Astronomy, Brigham Young University, Provo, UT, USA

To cite this Article Bruque, N. , Pandey, R. R. , Lake, R. K. , Wang, H. and Lewis, J. P.(2005) 'Electronic transport through a CNT-Pseudopeptide-CNT hybrid material', Molecular Simulation, 31: 12, 859 — 864
To link to this Article: DOI: 10.1080/08927020500323879
URL: http://dx.doi.org/10.1080/08927020500323879

Molecular Simulation, Vol. 31, No. 12, 15 October 2005, 859–864

Taylor & Francis
Taylor & Francis Group

Electronic transport through a CNT-Pseudopeptide-CNT hybrid material

N. BRUQUE†, R. R. PANDEY†*, R. K. LAKE†, H. WANG‡ and J. P. LEWIS‡

†Department of Electrical Engineering, University of California, Riverside, CA 92521, USA
‡Department of Physics and Astronomy, Brigham Young University, Provo, UT 84602, USA

(Received August 2005; in final form August 2005)

We present electron transmission studies on a pseudopeptide fragment (P) linking two (10,0) semi-infinite carbon nanotubes (CNTs). Calculations are performed using the non-equilibrium Green function formalism (NEGF) implemented within the tight-binding molecular dynamics density functional theory code FIREBALL. Results are compared with the transmission for an ideal (10,0) infinite CNT and a hydrogen passivated CNT-pseudopeptide-CNT (CNT–P–CNT) structure. The transmission spectrum indicates that the pseudopeptide fragment acts as a good bridge for hole transfer and strongly suppresses electron transfer.

Keywords: NEGF; Fireball; DFT; Electron-transfer; CNT; Peptide

1. Introduction

There is currently intense interest in chemical and bio-assembled nanosystems bringing together disparate materials such as metals, semiconductor nanocrystals, DNA, peptide nucleic acid (PNA), proteins, peptides and CNTs [1–3]. These systems tend to be large compared to the benzene dithiol (BDT) family of molecules studied heavily for molecular electronics [4–9]. There has been progress in moving beyond BDT for conduction studies and device modeling. However, to the best of our knowledge rotaxanes [10] and the metal-semiconducting carbon nanotube interface [11,12] are the largest systems to have been investigated for their conduction properties using *ab initio* models. We are interested in the electron transport through CNTs connected via short DNA and PNA oligomers and peptide linkers using density functional theory in conjunction with the non-equilibrium Green function (NEGF) formalism [4,7,13–20]. For the reason of system size, we have chosen to implement the NEGF algorithm within the tight binding *ab initio* DFT code FIREBALL [21,22], which has the demonstrated ability to model large bio-molecules [23]. We present an application of the NEGF code in FIREBALL to calculate the transmission spectrum through a CNT-pseudopeptide-CNT (CNT–P–CNT) hybrid structure shown in figure 1, which consists of a pseudopeptide fragment sandwiched between two (10,0) three unit cell zig-zag CNTs. This structure closely resembles the pseudopeptide backbone of PNA which is of interest for bio-assembly [24,25].

2. Method of calculation

The CNT–P–CNT structure shown in figure 1 is optimized using the MMX forcefield method built-in the PCMODEL software [26]. A section of the optimized structure is shown in figure 2, with the bond-lengths, bond angles and dihedral angles. The two benzene rings represent the portion of the two CNTs to which the pseudopeptide is attached. The optimized structure is then ported to FIREBALL where the BLYP exchange-correlation functional [27,28] is used to perform a single-point self-consistent calculation using a generalization of the Foulkes [29,30] energy functional referred to as DOGS after the authors of the original paper [31,32].

After the FIREBALL DFT calculation finishes, the device Hamiltonian, the overlap matrix and the device-to-contact coupling matrices are extracted. The spatial extent of the non-zero matrix elements (the sparsity of the matrices) is determined by the pseudopotential cutoff limits and the FIREBALL orbital radii. The matrices are

*Corresponding author. Email: raj@ee.ucr.edu

Molecular Simulation
ISSN 0892-7022 print/ISSN 1029-0435 online © 2005 Taylor & Francis
http://www.tandf.co.uk/journals
DOI: 10.1080/08927020500323879

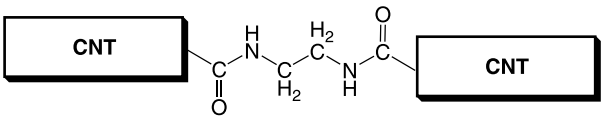

Figure 1. Schematic of the CNT–P–CNT structure used in this study.

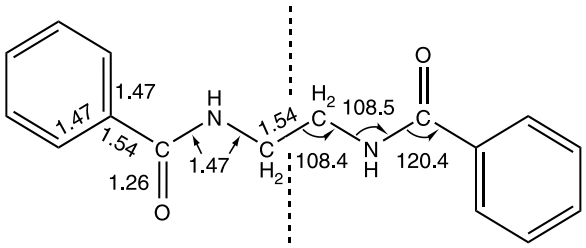

Figure 2. Geometrical parameters for a section of the CNT–P–CNT structure. The benzene rings represent the portion of the two CNTs to which the pseudopeptide is attached. The bond-lengths are represented in angstroms (°A) and the angles in degrees. Taking advantage of the symmetrical structure, the bond lengths are shown on left hand side of the dotted vertical line while the angles are shown on the right hand side to avoid crowding. Dihedral angles: $C_{CNT} - C_{CARBONYL} - N - C_{METHYLENE} = 145.0°$ and $C_{CARBONYL} - N - C_{METHYLENE} - C_{METHYLENE} = 62.0°$.

ported to the NEGF algorithm as a post-processor to the FIREBALL code.

One improvement that we have made over other implementations of NEGF with *ab initio* codes [4,7,13–20], is that we pre-calculate the surface self-energies for a given material, store them and access them as a look-up table during the NEGF calculation. This speeds up the NEGF calculation by over an order of magnitude.

In the initial DFT calculations of the CNT–P–CNT structure using FIREBALL, the CNTs on either end consist of 3 unit cells. For the NEGF calculation, the outside unit cell of each CNT is thrown away, and the self-energy matrices Σ^{ℓ} and Σ^{r} are added onto the new outside unit cell of the truncated CNTs as indicated in figure 3. These self-energies turn the finite CNTs into surfaces of semi-infinite CNTs. This same approach was used in calculating the transmission coefficients of the infinite (10,0) CNT shown in figure 4 to verify that truncation of one unit cell was sufficient to suppress spurious infinite size effects on the matrix elements extracted from FIREBALL. The FIREBALL orbitals of the atoms lying between the two dotted lines in figure 3 constitute the device and determine the size of the matrix $[E–H_D–\Sigma^{\ell}–\Sigma^{r}]$ which is the starting point of the NEGF calculations. The device matrix size is 678 which represents the total number of orbitals present.

We will describe the theory for calculating the surface self-energies and transmission of an ideal (10,0) CNT since these CNTs act as the contacts for the system that we study below. The matrix elements extend four atomic layers which constitute exactly one unit cell of the (10,0) CNT. We label the unit cells such that cells $\{-\infty,\ldots,0\}$ lie in the left contact, cells $\{1,\ldots,N\}$ lie in the "device," and cells $\{[N+1),\ldots\infty\}$ lie in the right contact. The matrix elements of the Hamiltonian group into intra-cell subblocks $D_{i;i}$ and inter-cell subblocks $t_{i;i\pm1}$. We define effective off-diagonal matrix elements $\tilde{t}$ as $\tilde{t}_{i,j} = t_{i,j} - (E + i\eta)S_{i,j}$ where $S_{i,j}$ is the overlap matrix element between non-orthogonal orbitals i and j, E is the energy, and η is a convergence factor that is non-zero only in the contacts. For calculations presented below, $\eta = 10\,\text{meV}$.

The calculation of the self-energy representing the semi-infinite CNT, begins with the calculation of the surface Green function. The surface Green function of the semi-infinite lead on the left $g^{r}_{0,0}$ is calculated from the self-consistent expression:

$$g^{r}_{0,0} = \left[(E + i\eta)S_{0,0} - D_{0,0} - \tilde{t}_{0,-1}g^{r}_{0,0}\tilde{t}_{-1,0}\right]^{-1} \qquad (1)$$

The convergence of this self-consistent calculation depends on the energy E. When the energy lies within a band-gap of the lead material, equation (1) converges quickly within five iterations. When the energy E lies in a band, convergence can be quite slow, taking up to 500 iterations with $\eta = 10\,\text{meV}$ and a convergence criteria of a 0.0001% difference change of the sum of the magnitude of all of the elements of $g^{r}_{0,0}$. We update by taking the average of the old and new value of $g^{r}_{0,0}$. The non-zero blocks of the self-energy matrices are calculated using

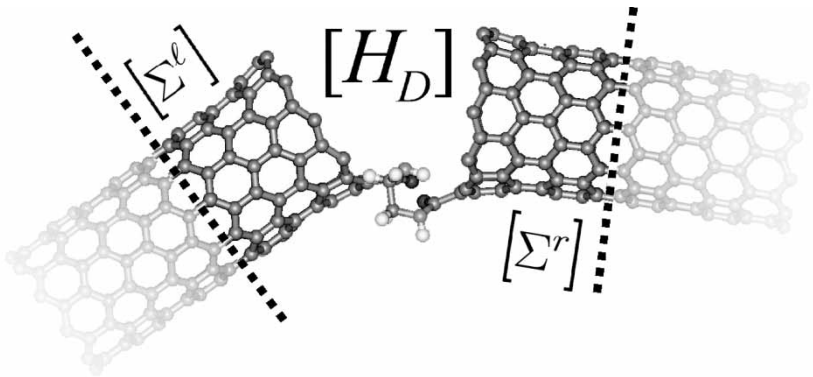

Figure 3. Relaxed CNT–P–CNT structure.

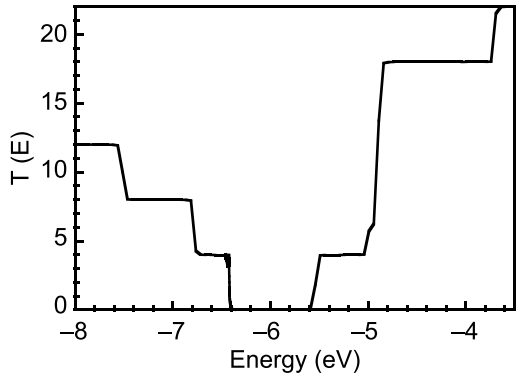

Figure 4. Transmission of a (10,0) CNT calculated with the matrix elements extracted from FIREBALL.

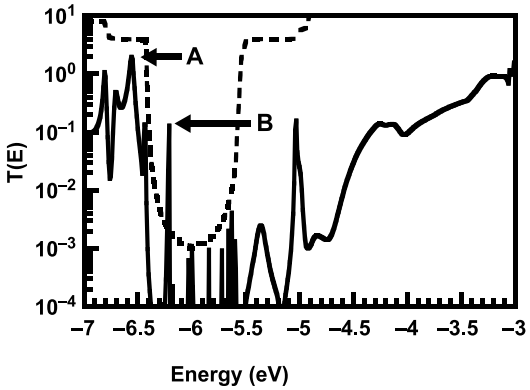

Figure 5. Transmission of CNT–P–CNT structure compared with (10,0) CNT.

$\Sigma^R_{1,1} = \tilde{t}_{1,0} g^R_{0,0} \tilde{t}_{0,1}$ and $\Sigma^R_{N,N} = \tilde{t}_{N,N+1} g^R_{N+1,N+1} \tilde{t}_{N+1,N}$. The energy-dependent matrices $\Sigma^R_{1,1}$ and $\Sigma^R_{N,N}$ are then stored for an array of energies for look-up during the transmission calculation. We will later refer to these self-energies as Σ^{ℓ} and Σ^{r}, respectively, indicating the left and right surface self-energies.

At each energy, the retarded Green function is calculated from

$$G^R(E) = [E - H_D - \Sigma^{\ell} - \Sigma^{r}]^{-1} \tag{2}$$

where the matrix H_D is constructed from orbitals lying on atoms that lie in the "device," i.e. unit cells $\{1,\ldots,N\}$ for the ideal CNT in the numbering scheme described above or the atoms lying between the dotted lines in figure 3. The transmission coeffcient is calculated from one of two equivalent expressions [33]

$$T(E) = \mathrm{tr}\left\{\Gamma^B_{1,1} G^R_{1,N} \Gamma^B_{N,N} G^R_{1,N}\right\} \tag{3}$$

or

$$T(E) = \mathrm{tr}\left\{\Gamma^{\mathrm{B}}_{1,1}\left[A_{1,1} - G^R_{1,1}\Gamma^B_{1,1} G^A_{1,1}\right]\right\} \tag{4}$$

where $\Gamma^B_{1,1} = i(\Sigma^{\ell} - \Sigma^{\ell\dagger})$, $\Gamma^B_{N,N} = i(\Sigma^{r} - \Sigma^{r\dagger})$, $A_{1,1} = i(G^R_{1,1} - G^A_{1,1})$ and $G^A = [\mathrm{G}^R]^{\dagger}$. Expression (3) is the more commonly known expression for transmission and corresponds to what has become known as the Fisher-Lee [34] form of the transmission coefficient although the expression was written down 10 years earlier by Caroli *et al.* [35]. Equation (4) is more numerically efficient since it only requires the calculation of the upper corner block of G^R.

One of the best verifications of the self-energy matrices is to calculate the transmission through an ideal periodic structure of the same material, in this case the (10,0) CNT. The transmission should turn on in integer steps at the valence band maximums and conduction band minimums. The integer turn-ons of the transmission shown in figure 4 match the band maxima and minima of the E-k band diagram calculated by FIREBALL as they should. The transmission is calculated using the look-up table of self-energies. For energies that do not lie on the stored array, the self-energies are linearly interpolated from the nearest two stored self-energies. Thus, figure 4 also verifies the correctness of our new self-energy look-up approach.

To understand the spatial extent of states at a given energy, we calculate and plot the covariant spectral function [36]

$$A_i(E) = -2\,\mathrm{Im}\,[\mathrm{tr}_i(SG^R(E)S)] \tag{5}$$

where the trace is over the basis states associated with atom i.

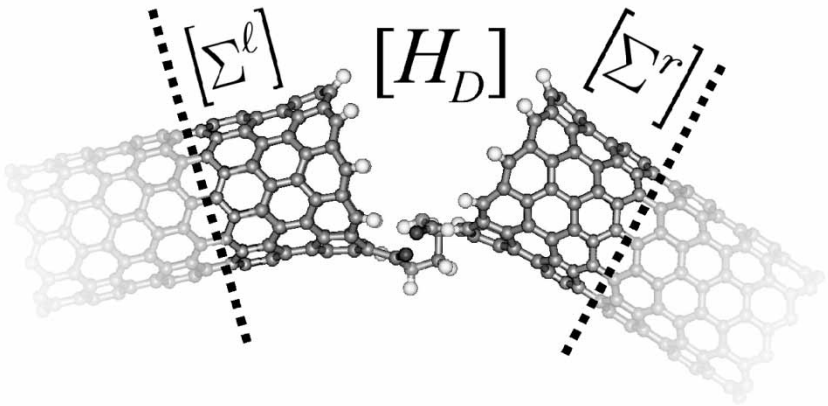

Figure 6. Relaxed CNT–P–CNT structure passivated with hydrogen atoms at the CNT-pseudopeptide interface.

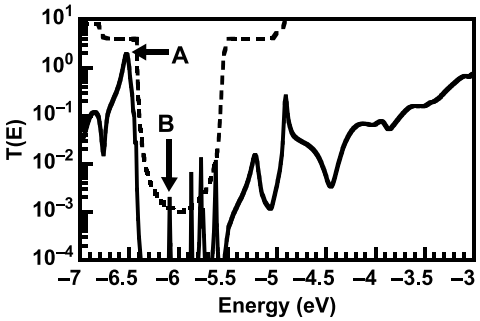

Figure 7. Transmission of passivated CNT–P–CNT compared with (10,0) CNT.

3. Results and discussion

Figure 5 shows a plot of the CNT–P–CNT transmission (solid line) overlaid on a plot of the bare CNT transmission (dashed line). The band-gap of the bare CNT begins at -6.5 eV and ends close to -5.5 eV. The peak transmission, seen at the edge of the valence band at approximately -6.56 eV (point A), indicates good hole transfer through CNT–P–CNT interface. Electron transmission from the conduction bands of the CNTs is strongly suppressed. The transmission resonances present within the CNT band-gap are attributed to the open orbitals present along the last layer of carbon atoms at the peptide CNT interface and to the states of the peptide. Approximately 1–2 min of wall clock time were required to calculate transmission at each energy on a stand-alone 3 GHz P4.

To reduce the transmission found within the bare CNT band-gap, the CNT–P–CNT structure is passivated with hydrogen atoms on each CNT as shown in figure 6. The device matrix size increases to 696 orbitals. The transmission plot shown in figure 7 still exhibits good hole transmission at the valence band edge and the strongest transmission peak at point B of figure 5 in the band-gap is gone. Electron transfer in the conduction band is still strongly suppressed.

A surface contour plot of the spectral function at point A of figure 7 is shown in figure 8. Even though this energy occurs within the valence band of the CNT, the wavefunction is strongly peaked on the O and N atoms of the pseudopeptide. The electron cloud of the CNT valence band can also be seen around the CNT leads.

A surface contour plot of the spectral function at point B of figure 6 is shown in figure 9. The state is confined to the pseudopeptide and exposed surface of the CNTs. There is no electron cloud further back in the CNT leads since this energy lies within the bandgap of the CNTs.

The transmission within the energies of the CNT bandgap is the result of resonant tunneling from the CNT end through the interface/peptide states out to the other CNT end. The imaginary potential, $\eta = 10$ meV, used when calculating the surface self-energies gives rise to a finite density of states in the bandgap of the CNT contacts and thus a finite Γ in equation (3) for energies within the CNT bandgap. This gives rise to the non-zero transmission in the bandgap. To diminish the remaining transmission resonances, the length of the CNTs should be greater. The transmission in the bandgap is exponentially dependent on the CNT length within the "device," i.e. $T(E) \sim e^{-2\kappa L_{\mathrm{CNT}}}$, where κ represents the evanescent wavevector in the band-gap of the CNTs. As the CNT lengths are increased within the "device" region, the resonant tunneling current observed in the bandgap will be exponentially suppressed.

4. Summary

A NEGF/DFT approach which uses look-up of precalculated surface self-energies is demonstrated. The look-up approach speeds up the NEGF calculation by over an order of magnitude. The approach is verified by calculating the transmission of an ideal, infinite (10,0) CNT. The approach is applied to the calculation of the transmission through a CNT-pseudopeptide-CNT structure. The results indicate that the peptide linker acts as a good bridge for hole transmission in the CNT valence

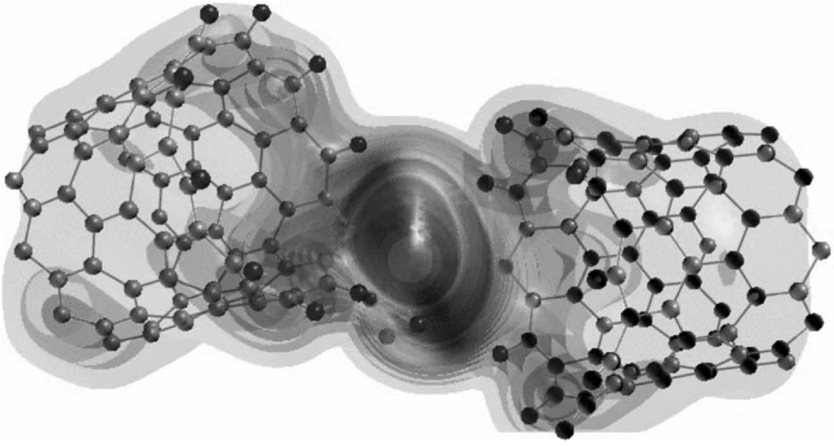

Figure 8. Point A: Contour surface plot of the spectral function at -6.53 eV near the valence band edge.

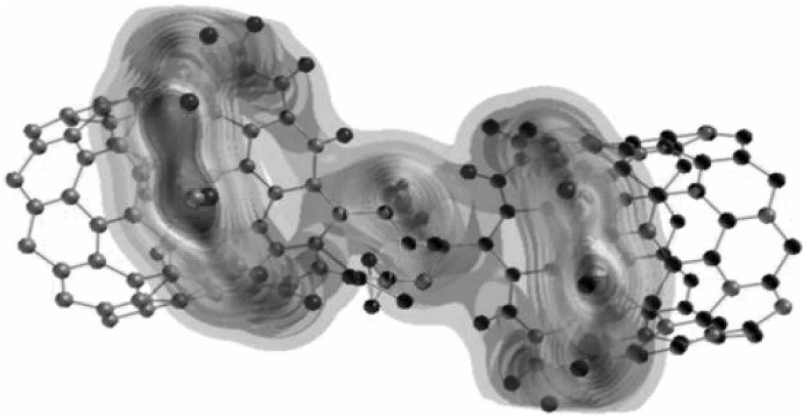

Figure 9. Point B: Contour surface plot of the spectral function at −5.87 eV inside the CNT bandgap.

band and strongly suppresses electron transmission in the CNT conduction band.

Acknowledgements

This work is supported by the Microelectronics Advanced Research Corporation Focus Center on Nano Materials (FENA), DARPA/DMEA-CNID (H94003-04-2-0404), and the NSF (DMR-0103248).

References

[1] E. Katz, I. Willner. Integrated nanoparticle-biomolecule hybrid systems: synthesis, properties, and applications. *Angew. Chem. Int. Ed.*, **43**, 6042 (2004).
[2] E. Katz, I. Willner. Biomolecule-functionalized carbon nanotubes: applications in nanobioelectronics. *Chem. Phys. Chem.*, **5**, 1085 (2004).
[3] W. Fritzsche (Ed.). *DNA-Based Molecular Electronics*, vol. 725, AIP, New York (2004).
[4] P. Damle, A. Ghosh, S. Datta. United description of molecular conduction: from molecules to metallic wires. *Phys. Rev. B*, **64**, 201403 (2001).
[5] P. Damle, A. Ghosh, S. Datta. First-principles analysis of molecular conduction using quantum chemistry software. *Chem. Phys.*, **281**(2–3), 171 (2002).
[6] T. Rakshit, G. Liang, A. Ghosh, S. Datta. Silicon-based molecular electronics. *Nano Lett.*, **4**, 1083 (2004).
[7] Y. Xue, S. Datta, M.A. Ratner. First-principles based matrix green's function approach to molecular electronic devices: general formalism. *Chem. Phys.*, **281**(2–3), 151 (2002).
[8] Y. Xue, S. Datta, M.A. Ratner. Charge transfer and band lineup in molecular electronic devices: a chemical and numerical interpretation. *J. Chem. Phys.*, **115**(9), 4292 (2001).
[9] S.N. Yaliraki, M.A. Ratner. Molecule-interface coupling effects on electronic transport in molecular wires. *J. Chem. Phys.*, **109**(12), 5036 (1998).
[10] W.-Q. Deng, R.P. Muller, W.A. Goddard. Mechanism of the stoddart-heath bistable rotaxane molecular switch. *J. Am. Chem. Soc.*, **126**, 13562 (2004).
[11] J.R. Reimers, A. Bilic, Z.-L. Cai, M. Dahlbom, N.A. Lambropoulos, G.C. Solomon, M.J. Crossley, N.S. Hush. Molecular electronics: from basic chemical principles to photosynthesis to steady-state through-molecule conductivity to computer architectures. *Aust. J. Chem.*, **57**, 1133 (2004).
[12] Y. Xue, M.A. Ratner. Scaling analysis of schottky barriers at metal-embedded semiconducting carbon nanotube interfaces. *Phys. Rev. B*, **69**(16), 161402 (2004).
[13] P.A. Derosa, J.M. Seminario. Electron transport through single molecules: scattering treatment using density functional green function theories. *J. Phys. Chem. B*, **105**(2), 471 (2001).
[14] Y. Xue, S. Datta, M.A. Ratner. Charge transfer and "band lineup" in molecular electronic devices: a chemical and numerical interpretation. *J. Chem. Phys.*, **115**(9), 4292 (2001).
[15] M. Brandbyge, J.-L. Mozos, P. Ordejón, J. Taylor, K. Stokbro. Density functional method for nonequilibrium electron transport. *Phys. Rev. B*, **65**(16), 165401/1–17 (2002).
[16] K. Stokbro, J. Taylor, M. Brandbyge, P. Ordejon. Transiesta—a spice for molecular electronics. *Mol. Electron. III Ann. N. Y. Acad. Sci.*, **1006**, 212 (2003).
[17] X. Zhang, L. Fonseca, A.A. Demkov. The application of density functional, local orbitals, and scattering theory to quantum transport. *Phys. Stat. Sol. (b)*, **233**(1), 70 (2002).
[18] J. Taylor, H. Guo, J. Wang. *Ab initio* modeling of quantum transport properties of molecular electronic devices. *Phys. Rev. B*, **63**(24), 245407/1–13 (2001).
[19] J. Heurich, J.C. Cuevas, W. Wenzel, G. Schön. Electrical transport through single-molecule junctions: from molecular orbitals to conduction channels. *Phys. Rev. Lett.*, **88**(25), 256803 (2002).
[20] J. Tomfohr, O.F. Sankey. Theoretical analysis of electron transport through organic molecules. *J. Chem. Phys.*, **120**(3), 1542 (2004).
[21] O.F. Sankey, D.J. Niklewski. *Ab initio* multicenter tight-binding model for molecular-dynamics simulations and other applications in covalent systems. *Phys. Rev. B*, **40**(6), 3979 (1989).
[22] J.P. Lewis, K.R. Glaesemann, G.A. Voth, J. Fritsch, A.A. Demkov, J. Ortega, O.F. Sankey. Further developments in the local-orbital density-functional-theory tight-binding method. *Phys. Rev. B*, **64**(19), 195103/1–10 (2001).
[23] J.P. Lewis, T.E.C. III, E.B. Starikov, H. Wang, O.F. Sankey. Dynamically amorphous character of electronic states in poly(da)-poly(dt) dna. *J. Phys. Chem. B*, **107**(11), 2581 (2003).
[24] K.A. Williams, P.T.M. Veenhuizen, B.G. de la Torre, R. Eritja, C. Dekker. Carbon nanotubes with dna recognition. *Nature*, **420**, 761 (2002).
[25] R. den Dulk, K.A. Williams, P.T.M. Veenhuizen, M.C. de Konig, M. Overhand, C. Dekker. Self-assembly experiments with pna-derivatized carbon nanotubes. In *DNA-Based Molecular Electronics*, W. Fritzsche (Ed.), vol. 725, pp. 25–31, AIP, New York (2004).
[26] *PCMODEL Version 9.00.0*. Serena Software (2004).
[27] A.D. Becke. Density-functional exchange-energy approximation with correct asymptotic behavior. *Phys. Rev. A*, **38**(6), 3098 (1988).
[28] C. Lee, W. Yang, R.G. Parr. Development of the colle-salvetti correlation energy formula into a functional of the electron density. *Phys. Rev. B*, **37**(2), 785 (1988).
[29] J. Harris. Simplified method for calculating the energy levels of weakly interacting fragments. *Phys. Rev. B*, **31**, 1770 (1985).
[30] W.M.C. Foulkes, R. Haydock. Tight-binding models and density-functional theory. *Phys. Rev. B*, **39**, 1252012536 (1989).
[31] A.A. Demkov, J. Ortega, O.F. Sankey, M.P. Grumbach. Electronic structure approach for complex silicas. *Phys. Rev. B*, **52**(3), 1618 (1995).

[32] O.F. Sankey, A.A. Demkov, W. Windl, J.H. Fritsch, J.P. Lewis, M. Fuentes-Cabrera. The application of approximate density functionals to complex systems. *Int. J. Quantum Chem.*, **69**, 327 (1998).

[33] R. Lake, G. Klimeck, R.C. Bowen, D. Jovanovic. Single and multiband modeling of quantum electron transport through layered semiconductor devices. *J. Appl. Phys.*, **81**(12), 7845 (1997).

[34] D.S. Fisher, P.A. Lee. Relation between conductivity and transmission matrix. *Phys. Rev. B*, **23**(12), 6851 (1981).

[35] C. Caroli, R. Combescot, P. Nozieres, D. Saint-James. Direct calculation of the tunneling current. *J. Phys. C: Solid State Phys.*, **4**, 916 (1971).

[36] D. Lohez, M. Lannoo. Generalization of the green's-functions formalism to nonorthogonal orbitals: application to amorphous SiO_2. *Phys. Rev. B*, **27**(8), 5007 (1983).